Capillary filling in open rectangular microchannels with spatially varying contact angle

Li-Hsuan Chang and Satish Kumar*

Department of Chemical Engineering and Materials Science, University of Minnesota, Minnesota, 55455, USA

Abstract

Capillary flow in microchannels is important for many technologies such as microfluidic devices, heat exchangers, and fabrication of printed electronics. Due to a readily accessible interior, open rectangular microchannels are particularly attractive for these applications. Here, we develop modifications of the Lucas-Washburn model to explore how a spatially varying contact angle influences capillary flow in open rectangular microchannels. Four cases are considered: (i) different uniform contact angles on channel sidewalls and channel bottom, (ii) contact angle varying along channel cross section, and (iii) contact angle varying monotonically along channel length, and (iv) contact angle varying periodically along channel length. For case (i), it is found that the maximum filling velocity is more sensitive to changes in the wall contact angle. For case (ii), the contact angles can be averaged to transform the problem to that of case (i). For case (iii), the time evolution of the meniscus position no longer follows the simple square-root law at short times. Finally, for case (iv), the problem is well described by using a uniform contact angle that is a suitable average. These results provide insight into how to design contact-angle variations to control capillary filling, and into the influence of naturally occurring contact-angle variations on capillary flow.

*E-mail: kumar030@umn.edu

Introduction

Capillary flow is an ubiquitous phenomenon seen in our daily lives, such as transport of water through plant stems and absorption of water through towels. Due to the attraction between a solid surface and liquid molecules, capillary forces pull liquid molecules from the liquid phase to the surface. The pressure jump across the curved interface that forms can cause capillary flow. Microchannels are channels with width ranging from 1 mm to 1 μ m. In these channels, capillary forces are important. Capillary flow in closed microchannels can be applied to microfluidic devices [1–3], heat exchangers [4–6], and microreactors [7–9]. In microfluidic devices and microreactors, microchannels enable reactions to become safe and controllable while providing rapid mixing [10–12]. Also, heat transfer systems can be made lighter and with a higher heat transfer coefficient by using microchannels [13–15].

Compared with capillary flow in closed microchannels, capillary flow in open microchannels offers distinct advantages. Since the channel is open to the atmosphere, nanoparticles can be deposited in microchannels by evaporating a colloidal suspension. This strategy has been applied to the fabrication of printed electronic devices, such as conductors, resistors and low-pass filters [16–18], where open rectangular microchannels were used due to their ease of fabrication. Printed electronic devices are of considerable technological importance since they are low-cost, flexible, and light [19–21]. Additionally, open rectangular microchannels appear in microfluidic devices for applications such as heat pipes [22, 23] and artificial lungs [24]. Therefore, due to the importance of capillary filling in open rectangular microchannels for printed electronic devices and microfluidic devices, it is desirable to have a fundamental understanding of capillary filling in this geometry.

Yang et al. [25] developed a modified Lucas-Washburn equation to describe the time evolution of the meniscus position in open rectangular microchannels. This model is based on the Lucas-Washburn model, which is for capillary filling in closed microchannels [26–33]. In the Lucas-Washburn model, it is assumed that the liquid front is a circular-arc meniscus,

which causes a capillary-pressure gradient and makes liquid flow into the microchannel. Viscous forces resist the flow. However, for capillary filling in open microchannels, there is an upper liquid-air interface. To deal with this interface, Yang et al. [25] assumed a flat upper liquid-air interface and used the free-energy change as the liquid advances along the open microchannel to calculate the capillary force. By using this model, they found that a lower equilibrium contact angle causes faster capillary filling, which is consistent with experimental observations. Later, Kolliopoulos et al. [34] developed a more accurate but more complex model based on lubrication theory, and also performed complementary experiments. They found that the modified Lucas-Washburn model of Yang et al. [25] provides quantitatively accurate predictions for larger channel aspect ratios (ratio of channel height to width) and larger contact angles.

Since capillary flow has many applications, it is desirable to understand how natural or engineered spatial variation of contact angle changes capillary flow in open microchannels. There are many approaches to modify surface wettability such as chemical deposition [35–38], laser ablation [39–41], lithographic patterning [42–44], and micromachining [41, 45, 46]. O'Loughlin et al. [47] used photocatalytic lithographic patterning to fabricate closed microchannels with periodic hydrophilic and hydrophobic regions along the channel length, and then performed capillary-rise experiments. They found that when the length of patterning is larger than the capillary length, liquid rises faster in hydrophilic segments. Also, Suk and Cho [48] used hydrophobic patterns to control the velocity of capillary flow in closed microchannels. From their experiment, they observed that increasing the fraction of the channel covered with hydrophobic patterns makes capillary flow slower. Therefore, we know that the dynamics of capillary flow is sensitive to this kind of surface heterogeneity.

Additionally, Xing et al. [49] used experiments and the Lucas-Washburn equation to explore capillary imbibition in an open semicircular copper channel with a wettability gradient. In their experiments, they used chemical treatment to create a spatially varying contact

angle. Notably, the decrease in contact angle produced by chemical treatment was accompanied by an apparent increase in surface roughness. From both their mathematical model and experiments, they observed that a positive wettability gradient along the channel length can enhance the velocity of capillary filling. Therefore, from previous research, we know that fabrication of microchannels with spatially varying contact angle is feasible and spatially varying contact angle can influence capillary flow.

Although previous studies show that a spatially varying contact angle can influence capillary flow, the underlying mechanisms are still not clear. For example, the study of Xing et al. created wettability gradients by changing surface roughness along the microchannel, which also changes viscous forces [49]. Therefore, in their study, the effects of spatially varying contact angle on capillary flow are not isolated. Additionally, in their mathematical model, they used the free-energy change of a droplet and the velocity profile in a closed circular microchannel to estimate the capillary and viscous forces in an open microchannel [49]. These assumptions are not expected to be accurate.

In the present work, we calculate these forces more accurately and isolate the influence of wettability gradients. We do this in the context of the modified Lucas-Washburn model because of its simplicity and versatility. We focus on the case of open rectangular microchannels because of their technological importance and ease of fabrication (as discussed above). Although the modified Lucas-Washburn model makes a number of assumptions, its predictions agree well with those from a more complex but more accurate model based on lubrication theory in the regime of larger channel aspect ratios and contact angles [34]. Outside of this regime, the modified Lucas-Washburn model still provides qualitatively accurate predictions of meniscus position, although it cannot capture the behavior of liquid fingers that form in the channel corners [34]. Nevertheless, the modified Lucas-Washburn model is still useful for building initial physical understanding of the problems we consider here, and the results we obtain are expected to motivate future work involving more detailed modeling

and complementary experiments.

In this work, we consider capillary filling in open rectangular microchannels with four different kinds of contact-angle variations: (i) different uniform contact angles on channel sidewalls and channel bottom, (ii) contact angle varying along channel cross section, (iii) contact angle varying monotonically along channel length, and (iv) contact angle varying periodically along channel length. The results from these four different cases suggest strategies to manipulate capillary filling by designing contact-angle variations and yield a fundamental understanding of the influence of naturally occurring contact-angle variations on capillary flow.

Results and Discussion

Capillary Filling with Two Different Contact Angles

In this section, we derive a modified Lucas-Washburn equation that includes the effects of spatially varying contact angle, where there are two different static contact angles, θ_w and θ_b on the walls and bottom, respectively (All angles in this work are given in degrees.)

A schematic is given in figure 1. The height and width of the microchannel are denoted

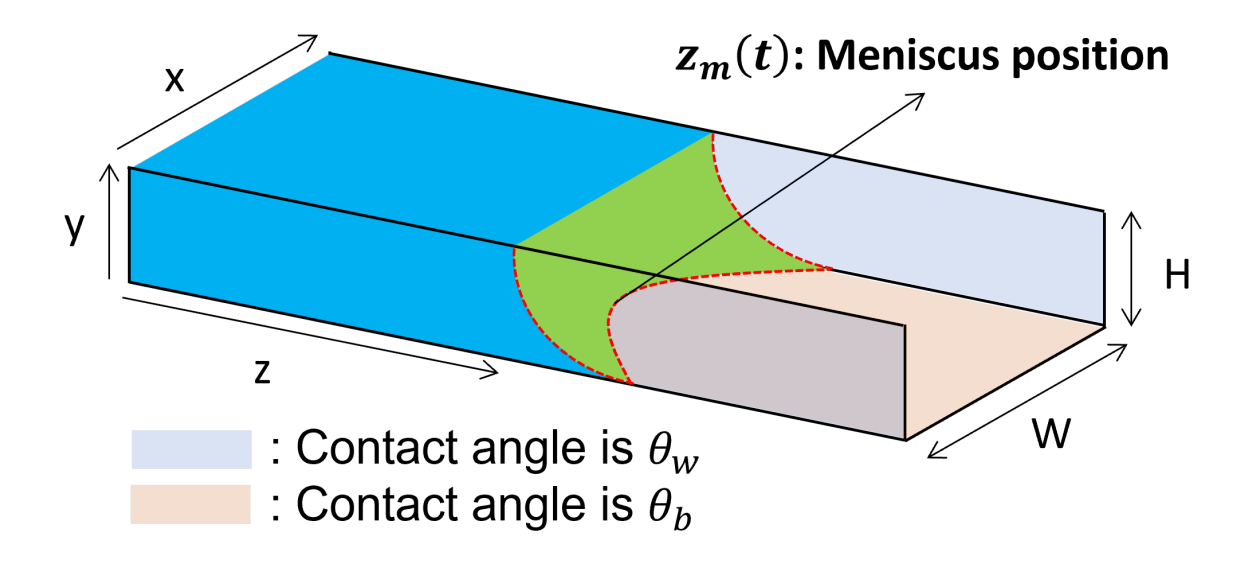


Figure 1: Schematic of capillary flow in an open rectangular microchannel with different contact angles on the walls and bottom.

by H and W, with the aspect ratio given by $\lambda = H/W$. The length of the microchannel is denoted by L. In figure 1, the meniscus position is denoted by z_m , and liquid fills the whole microchannel so the rate of change of z_m represents the velocity of capillary filling. In this paper, we consider the liquid to be incompressible and Newtonian with viscosity μ and surface tension σ . The liquid and solid are in contact with a gas (vapor) whose dynamics can be neglected.

We use $\rho H^2 U^2$, $\mu U L$, σH , and $\rho g L H^2$ to estimate the magnitudes of inertial, viscous, capillary, and gravity forces, respectively, where U is the magnitude of the velocity of capillary filling. By assuming that filling is dominated by capillary and viscous forces, we get $U \sim (\sigma H)/(\mu L)$. By using this expression and the force estimates given above, we see that when $(\rho U H^2)/(\mu L)$ (Reynolds number) and $\rho g L H/\sigma$ (Bond number) are much smaller than 1, we can neglect inertial and gravity forces. Under these conditions, we have

$$f_v + f_c = 0, (1)$$

where f_v and f_c are the viscous and capillary forces exerted on the liquid.

We also assume that the capillary number (ratio of viscous to surface-tension forces), $(\mu UL)/(\sigma H)$ is small, which allows for the use of capillary statics to describe the interface shape [34]. Additionally, any speed dependence of contact angle (i.e. the dynamic contact angle phenomenon) is expected to be negligible at low capillary numbers so that the contact angles are well described by their static values [50]. Indeed, for the case where the wall and bottom contact angles are the same, model predictions based on this simple assumption agree well with experimental observations in open rectangular microchannels [34].

To get f_v , we need to know the velocity field in the microchannel. By assuming a flat upper liquid-gas interface (the blue region in figure 1) and parallel flow down the microchannel, the velocity vector only has a z-component, u(x, y). By neglecting inertial and gravity forces, we simplify the z-component of the momentum conservation equation to get

$$\frac{\partial^2 u}{\partial x^2} + \frac{\partial^2 u}{\partial y^2} = \frac{1}{\mu} \frac{dp}{dz},\tag{2}$$

where p is the pressure in the liquid. Boundary conditions are given by a no-stress condition at the liquid-gas interface, which is

$$\frac{\partial u}{\partial y} = 0, \quad \text{at } y = H$$
 (3)

and a no-slip condition at the walls and bottom of the microchannel:

$$u = 0$$
, at $x = \frac{-W}{2}$, $\frac{W}{2}$ and $y = 0$. (4)

By using separation of variables, Ouali et al. [51] solved equations (2), (3), and (4) and got u(x,y). By integrating the shear stress on surface of the microchannel, one obtains the expression for the viscous force, which is

$$f_v = -\mu z_m \left(\int_{-\frac{W}{2}}^{\frac{W}{2}} \frac{\partial u}{\partial y} \Big|_{y=0} dx + 2 \int_0^H \frac{\partial u}{\partial x} \Big|_{x=\frac{W}{2}} dy \right).$$
 (5)

In this system, since we assume a constant-curvature front, the average velocity of the fluid, u_{ave} , equals the rate of change of z_m , which is

$$u_{ave} = \frac{\int_{-\frac{W}{2}}^{\frac{W}{2}} \int_{0}^{H} u(x, y) dy dx}{HW} = \frac{dz_{m}}{dt}.$$
 (6)

By inserting the exact expression of u(x, y) and equation (6) into equation (5), we get the viscous force in open rectangular microchannels, which is

$$f_v = -\frac{3\mu z_m}{\lambda \xi(\lambda)} \frac{dz_m}{dt},\tag{7}$$

where $\xi(\lambda)$ is a function of the aspect ratio [51]. Note that equation (7) has the same form as the viscous force without any contact-angle variation.

We now consider the capillary force. When liquid flows spontaneously into an open rectangular microchannel, the area of solid-gas (vapor) interface decreases and the interfacial free energy decreases consequently. Therefore, the capillary force is calculated by the reduction of interfacial free energy due to the liquid coverage on the surface of the microchannel [52],

$$f_c = -\frac{dG}{dz_m},\tag{8}$$

where G is the free energy of the liquid in the microchannel. In this system, the interfacial free energy is composed of liquid-gas, solid-liquid and solid-gas interfacial free energies,

$$G = \int_{A_{SL}} \sigma_{SL} dA' + \int_{A_{SV}} \sigma_{SV} dA' + \int_{A_{LV}} \sigma dA', \tag{9}$$

where σ , σ_{SL} , and σ_{SV} are liquid-gas, solid-liquid and solid-gas surface tensions. A_{LV} , A_{SL} , and A_{SV} are the areas of liquid-gas, solid-liquid, and solid-gas interfaces. By assuming a constant-curvature front and flat upper liquid-gas interface (the green and blue regions in figure 1), we get $G = 2Hz_m(\sigma_{SL} - \sigma_{SV}) + Wz_m(\sigma_{SL} - \sigma_{SV}) + Wz_m\sigma$. Since the microchannel has two different contact angles on the walls and bottom, by using Young's equation,

$$\sigma_{SV} - \sigma_{SL} = \sigma \cos(\theta_0), \tag{10}$$

where θ_0 is the static contact angle, we get $G = -\sigma W z_m \cos(\theta_b) - 2\sigma H z_m \cos(\theta_w) + \sigma W z_m$. By inserting this into equation (8), we get

$$f_c = \sigma W(\cos(\theta_b) + 2\lambda \cos(\theta_w) - 1). \tag{11}$$

Finally, by inserting equations (7) and (11) into equation (1), we get the modified Lucas-

Washburn equation for capillary filling in open rectangular microchannels with two different contact angles,

$$\frac{2H\sigma\xi(\lambda)(\cos(\theta_b) + 2\lambda\cos(\theta_w) - 1)t}{3\mu} = (z_m)^2.$$
 (12)

From equation (12), we see that decreasing μ and increasing σ increase the velocity of capillary filling. Larger viscosity makes it harder for the liquid to flow so capillary filling becomes slower. On the other hand, by the Young-Laplace equation, larger surface tension makes the pressure difference between the liquid front and gas phase larger so capillary filling becomes faster.

For convenience, we non-dimensionalize as follows,

$$\widetilde{t} = \frac{2H\sigma t}{\mu L^2}, \quad \bar{z}_m = \frac{z_m}{L},$$
(13)

where L is length of the microchannel. By inserting equation (13) into equation (12), we get a dimensionless mobility which is

$$\hat{k}_z = \frac{\bar{z}_m}{\sqrt{\bar{t}}} = \sqrt{\frac{\xi(\lambda)(\cos(\theta_b) + 2\lambda\cos(\theta_w) - 1)}{3}}.$$
(14)

The dimensionless mobility, \hat{k}_z , is indicative of the efficiency of capillary filling since when \hat{k}_z is larger, we have faster capillary filling.

Figure 2 shows a plot of \hat{k}_z vs. λ when $\theta_w = \theta_b = 20^\circ$. From figure 2, we see that there is an aspect ratio which maximizes the mobility, which means for a given θ_w and θ_b , there is a λ_{max} that maximizes the velocity of capillary filling. The reason is that when the aspect ratio increases, the viscous force from walls increases and hinders capillary filling. On the other hand, when the aspect ratio decreases, the viscous force from the bottom increases and also hinders capillary filling. Therefore, to achieve fast capillary filling, we should use microchannels with an aspect ratio around the black point in figure 2.

 λ_{max} is important because it can tell us how to maximize the velocity of capillary filling. However, θ_w and θ_b change λ_{max} . Figure 3(a) shows the relation between θ_w , θ_b , and λ_{max} . From this figure, we see that when we increase both θ_w and θ_b , λ_{max} becomes larger. This is because when both θ_w and θ_b increase, the capillary force decreases. Therefore, we need a larger aspect ratio to increase the capillary force (see equation (11)) and maximize the velocity of capillary filling.

 $\hat{k}_{z,max}$ is the value of \hat{k}_z corresponding to λ_{max} . It is important since it is indicative of the maximum velocity of capillary filling for a given θ_w and θ_b . Figure 3(b) shows the relation between θ_w , θ_b , and $\hat{k}_{z,max}$. From this figure, we see that smaller θ_w and θ_b cause faster capillary filling because smaller θ_w and θ_b make the constant-curvature front more curved and increase the pressure difference between the constant-curvature front and gas phase. Also, from figure 3(b), we see that the upper left corner is darker than the lower right corner, which means $\hat{k}_{z,max}$ is more dependent on θ_w . From figure 3(a), λ_{max} is always larger than 0.5, which means the area of the walls is larger than the area of the bottom, so compared with decreasing θ_b , decreasing θ_w reduces the interfacial free energy more. Therefore, to enhance the velocity of capillary filling, decreasing θ_w is better than decreasing

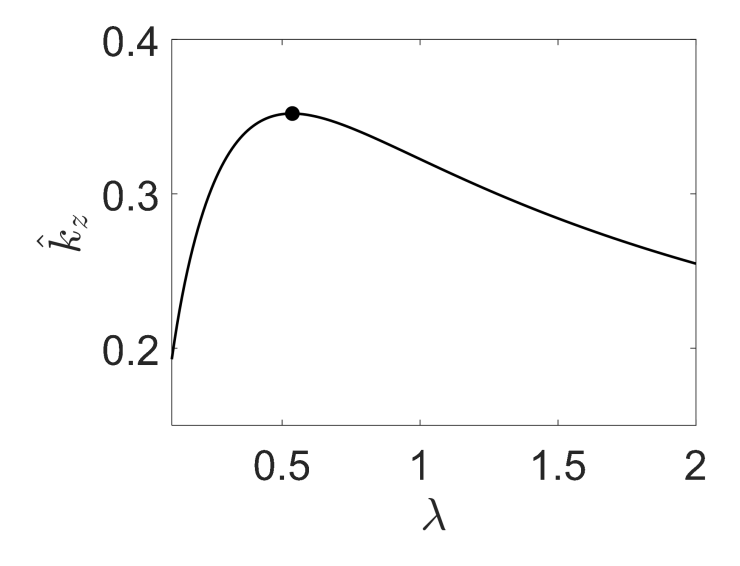


Figure 2: \hat{k}_z as a function of λ when $\theta_w = \theta_b = 20^{\circ}$.

 θ_b . For larger θ_w and θ_b , we need to use microchannels with a higher aspect ratio to maximize the velocity of capillary filling.

Contact-Angle Variation along Cross Section

Previously, we determined how wall and bottom contact angles influence the velocity of capillary filling. However, in experiments, it is hard to have microchannels with two completely different contact angles on the walls and bottom so we want to consider the more general case where the equilibrium contact angle, θ_0 , is a function of position along the cross section. The viscous force is again given by equation (7). For the capillary force, we need to calculate the interfacial free energy, G. By using equation (9) and assuming a constant-curvature front and flat upper liquid-gas interface, we get $G = z_m(2\int_0^H (\sigma_{SL} - \sigma_{SV})dH' + \int_{-\frac{W}{2}}^{\frac{W}{2}} (\sigma_{SL} - \sigma_{SV})dW' - W\sigma)$. Since there is a contact-angle variation along the cross section, by using equation (10), we get $G = -z_m(2\int_0^H \sigma\cos\theta_0 dH' + \int_{-\frac{W}{2}}^{\frac{W}{2}} \sigma\cos\theta_0 dW' - W\sigma)$. By inserting this into equation (8), we get

$$f_c = \sigma(2\int_0^H \cos\theta_0 dH' + \int_{-\frac{W}{2}}^{\frac{W}{2}} \cos\theta_0 dW' - W). \tag{15}$$

From equation (15), we see that the capillary force is composed of three parts which

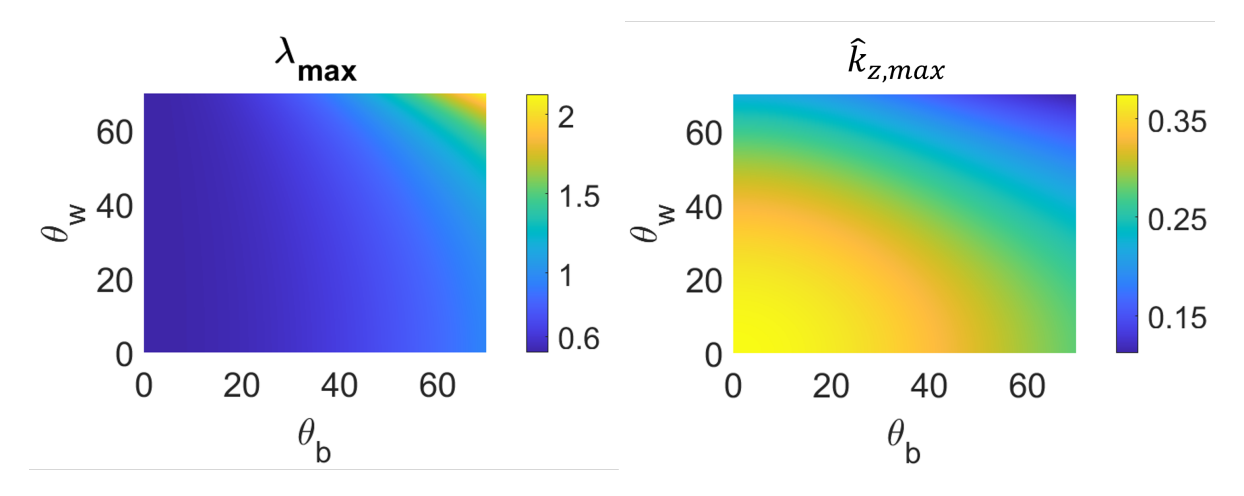


Figure 3: (a) The aspect ratio that maximizes the velocity, λ_{max} , and (b) maximum dimensionless mobility, $\hat{k}_{z,max}$, for different θ_w and θ_b .

are the interfacial free-energy change on the walls, the interfacial free-energy change on the bottom and the liquid-gas interfacial free energy. To understand how contact-angle variation changes the capillary force, we use average contact angles $\theta_{w,ave}$ and $\theta_{b,ave}$, where $\theta_{w,ave}$, $\theta_{b,ave}$ are defined as

$$H\cos(\theta_{w,ave}) = \int_0^H \cos\theta_0 dH' \text{ and } W\cos(\theta_{b,ave}) = \int_{-\frac{W}{2}}^{\frac{W}{2}} \cos\theta_0 dW'.$$
 (16)

By inserting equation (16) into equation (15), we simplify the expression of f_c ,

$$f_c = \sigma W(\cos(\theta_{b,ave}) + 2\lambda\cos(\theta_{w,ave}) - 1). \tag{17}$$

Also, we rearrange equation (16) and get explicit forms of $\theta_{w,ave}$ and $\theta_{b,ave}$, which are

$$\theta_{b,ave} = \cos^{-1} \left(\frac{\int_{-\frac{W}{2}}^{\frac{W}{2}} \cos \theta_0 dW'}{W} \right), \theta_{w,ave} = \cos^{-1} \left(\frac{\int_0^H \cos \theta_0 dH'}{H} \right). \tag{18}$$

These relationships are analogs of the Cassie equation, which is used to predict effective contact angles on chemically heterogeneous surfaces [53].

Finally, by inserting equations (7) and (17) into equation (1), we get the modified Lucas-Washburn equation for capillary filling in microchannels with contact-angle variation along the cross section,

$$\frac{2H\sigma\xi(\lambda)(\cos(\theta_{b,ave}) + 2\lambda\cos(\theta_{w,ave}) - 1)t}{3\mu} = (z_m)^2.$$
 (19)

We see that equation (19) is similar to equation (12), which means that the effect of contact-angle variation along the cross section can be described in terms of spatially averaged contact angles. Therefore, the conclusions of the previous section can be applied to this kind of contact-angle variation, using equation (18) to obtain the averaged contact angles.

Contact-Angle Variation along Channel Length

We now consider the case where the contact angle varies along the channel length. The viscous force is again given by equation (7). Compared with the cases considered previously, the shape of the liquid front changes with meniscus position since contact angle varies along the channel length. To simplify the model, we assume that the length of capillary filling is much larger than the length of the liquid front. Therefore, when the liquid flows through the microchannel, the free-energy change from capillary filling is much larger than that from the small liquid front.

By neglecting the free-energy change at the small liquid front and assuming a flat upper liquid-gas interface, from equation (9), we get $G = \int_0^{z_m} (\sigma_{SL} - \sigma_{SV})(2H + W) + \sigma W dz'$. After that, by using equation (10), we get $G = \int_0^{z_m} \sigma(W - (2H + W)\cos(\theta_0))dz'$, where θ_0 is the equilibrium contact angle, which varies along the microchannel. By inserting this expression into equation (8), we get the capillary force, which is

$$f_c = \sigma W((2\lambda + 1)\cos(\theta_0) - 1), \tag{20}$$

where λ is aspect ratio. By inserting equations (7) and (20) into equation (1), we obtain the modified Lucas-Washburn equation for capillary filling in microchannels with contact-angle variation along the z-direction,

$$\frac{H\sigma\xi(\lambda)t}{3\mu} = \int_0^{z_m} \frac{z}{(1+2\lambda)\cos(\theta_0(z)) - 1} dz. \tag{21}$$

To gain additional insight, we non-dimensionalize as follows,

$$\bar{t} = \frac{H\sigma\xi(\lambda)t}{3\mu l^2}, \quad \bar{z} = \frac{z}{l}, \quad \bar{z}_m = \frac{z_m}{l},$$
(22)

where l is the length scale of the contact-angle variation. By inserting equation (22) into

equation (21), we get a dimensionless modified Lucas-Washburn equation with contact-angle variation along the channel length,

$$\bar{t} = \int_0^{\bar{z}_m} \frac{\bar{z}}{(1+2\lambda)\cos(\theta_0(\bar{z})) - 1} d\bar{z}.$$
 (23)

From equation (23), we see that if θ_0 does not vary along the channel length, by using equations (22) and (14), we can reduce equation (23) back to the modified Lucas-Washburn equation without any contact-angle variation [25].

To see how contact-angle variation along the channel length influences the velocity of capillary filling, we consider six different cases, which are shown in figures 4(a) and 4(c). In cases 1, 2, and 3, we increase, fix and decrease the contact angle from the start of the channel, respectively, so that all contact angles eventually approach the same value. In cases 4, 5, and

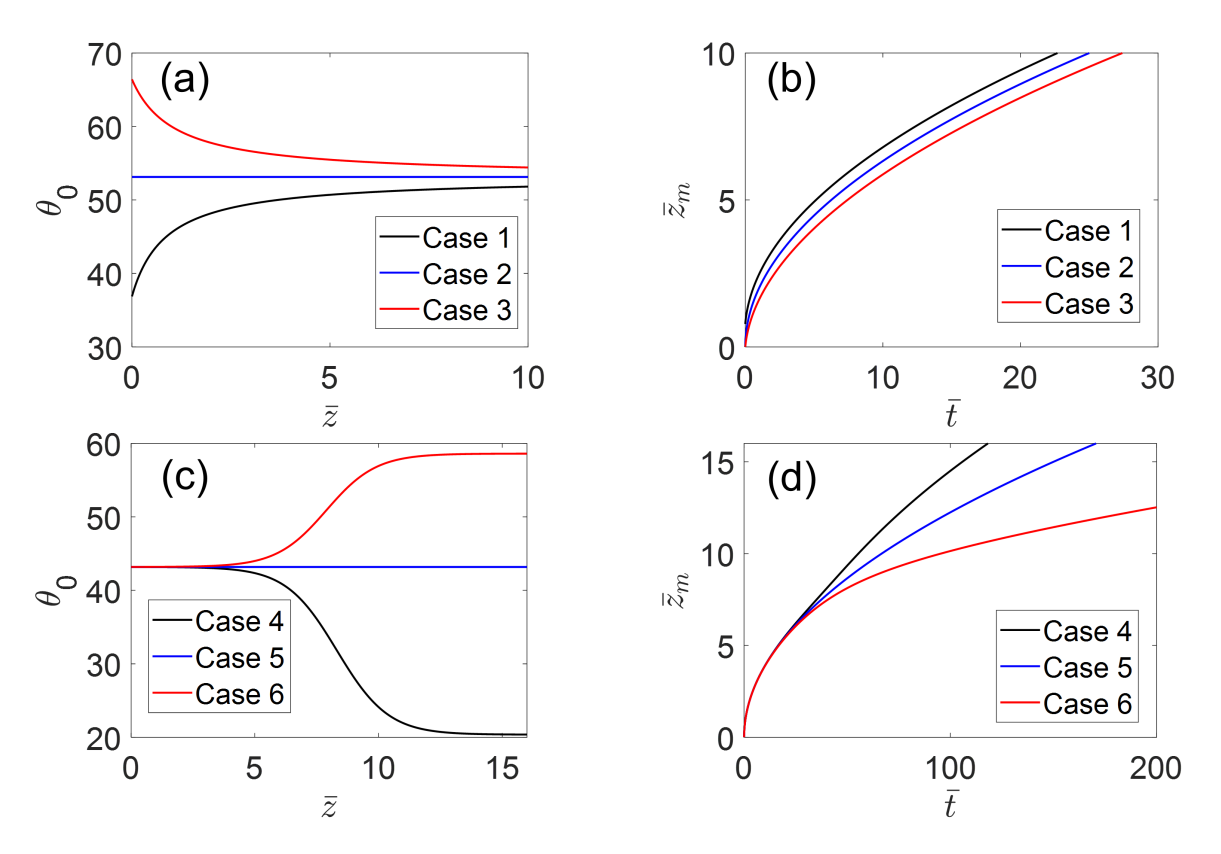


Figure 4: θ_0 vs. \bar{z} and \bar{z}_m vs. \bar{t} when $\lambda = 2$ with (a, b) contact-angle variations for cases 1-3 and when $\lambda = 0.7$ with (c, d) contact-angle variations for cases 4-6.

6, we keep the contact angle the same at the start of the channel and then decrease, fix, and increase contact angle, respectively. The analytical relation between the contact angle and position in figures 4(a) and 4(c) are equations (A.1) and (A.3) in the appendix. By using equation (21), we get figures 4(b) and 4(d), and the analytical relations between \bar{z}_m and \bar{t} are equations (A.2) and (A.4) in the appendix.

From figures 4(a) and 4(b), we see that capillary filling without a wettability gradient (case 2) is faster than capillary filling with a positive wettability gradient (case 3). This is in contrast to the experiments of Xing et al. discussed in the introduction. In their experiments, they compared capillary filling in open microchannels having (i) a contactangle variation from 45° to 3° and (ii) a constant contact angle of 3°. They observed that capillary filling in the channel with the wettability gradient was faster. In their experiments, they decreased contact angle by chemical treatment, and attributed the decrease in contact angle to an increase in surface roughness. Our results suggest that the surface roughness in their experiments slows down capillary filling and outweighs the influence of having a low wettability throughout the channel. Since surface roughness is not incorporated into our model, we are able to isolate the influence of wettability gradients.

From figure 4(b), we see that at long times, the difference between the meniscus positions is approximately the same. The reason is that if the contact angle variation primarily occurs at the beginning of the microchannel (figure 4(a)), then the velocity of capillary filling will be similar much further down the channel. Also, from figures 4(c) and 4(d), we see that if the contact angle gradually changes to different value, the meniscus positions tend to diverge at long times. This divergence is due to different capillary forces far away from the microchannel entrance. Note that at long times, \bar{t} is still proportional to \bar{z}_m^2 in all cases (see Appendix), although this proportionality does not hold at short times.

Finally, we briefly comment on the potential importance of inertial effects. An orderof-magnitude analysis of the modified Lucas-Washburn equation that accounts for inertial effects (see Appendix) indicates that inertial effects are important over a length scale $L^* \sim \sqrt{\rho \sigma H^3}/\mu$. Thus, inertial effects are expected to be negligible when the length scale of the wettability variation is much larger than L^* . Using the data from the experiments reported in Ref. [34], values of L^* can range from $\sim 0.1~\mu m$ to $\sim 1~mm$. For the cases considered previously where the contact angle varies along the channel cross section, inertial effects are not expected to be important since the flow is in the axial direction.

Periodic Contact-Angle Variation along Channel Length

We next consider a periodic contact-angle variation composed of two different contact angles, θ_1 and θ_2 . A schematic is given in figure 5, where ϵ is the period length. Since θ_0 is a periodic function, we expect from equation (23) that \bar{t} will have oscillations with period ϵ . Of practical interest is a mean time for capillary filling, which we denote as \bar{t}_a and develop an expression for below.

Although inertial effects may be important near the regions where the contact angle changes from one value to the other, we expect that such effects should not significantly affect the long-time meniscus behavior if the period length is much larger than the length scale over which inertial effects are important, L^* (see previous section). Moreover, neglecting inertial effects allows us to isolate the influence of wettability gradients from those of inertia, leading

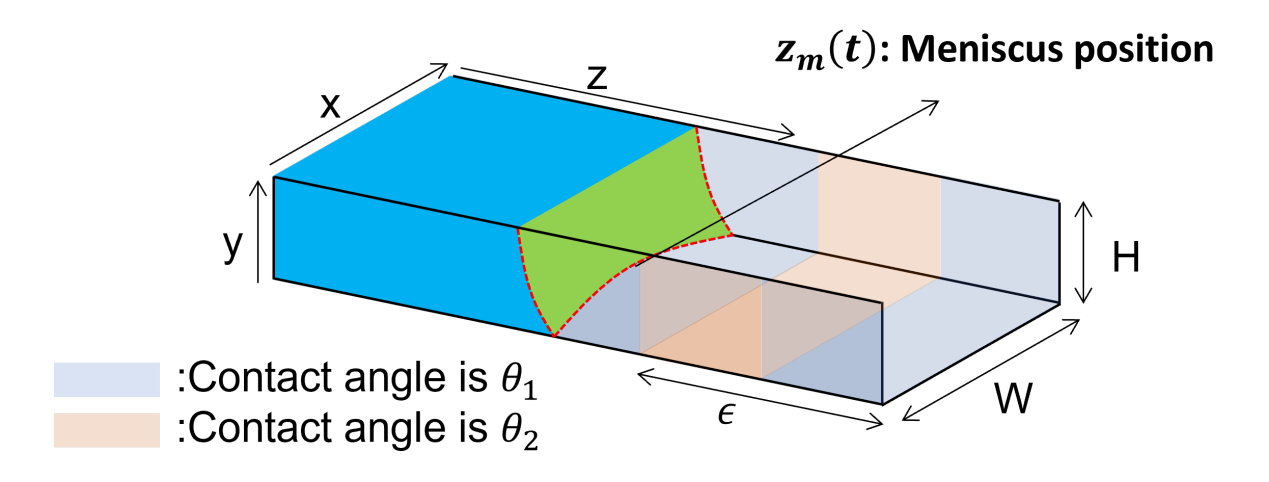


Figure 5: Schematic of capillary flow in an open rectangular microchannel with periodic contact-angle variation.

to the development of simple analytical expressions that provide physical insight. The results from the model we develop here serve as motivation for future work involving the development of more complex models that account for inertial effects and test the assumptions made here.

We first derive an expression for $d\bar{t}_a/d\bar{z}$. Assuming $\bar{t}_a \simeq \bar{t}$, by using the fundamental theorem of calculus and equation (23), we get

$$\int_0^{\bar{z}_m} \frac{d\bar{t}_a}{d\bar{z}} d\bar{z} \simeq \int_0^{\bar{z}_m} \frac{\bar{z}}{(1+2\lambda)\cos(\theta_0(\bar{z})) - 1} d\bar{z}.$$
 (24)

In this system, there are two different length scales, which are L, the length scale of the microchannel, and ϵ , the length scale of the period. Since L is much larger than ϵ , it is useful to define a length scale between L and ϵ , which we denote as Δz . We define $\Delta z = n\epsilon$ such that $\epsilon/L \ll \Delta z/L = \Delta \bar{z} \ll 1$, where n is a integer. Since $\frac{d\bar{t}_a}{d\bar{z}}$ and \bar{z} do not change significantly over $\Delta \bar{z}$ and that only θ_0 changes significantly in this region, for the integral in equation (24) on each small segment with length $\Delta \bar{z}$, we can pull $\frac{d\bar{t}_a}{d\bar{z}}$ and \bar{z} out of the integral and retain the $\cos(\theta_0)$ term in the integral, which leads to

$$\frac{d\bar{t}_a}{d\bar{z}}|_{\bar{z}=\bar{z}_m}\Delta\bar{z}\simeq\bar{z}_m\int_{\bar{z}_m-\Delta\bar{z}}^{\bar{z}_m}\frac{1}{(1+2\lambda)\cos(\theta_0(\bar{z}))-1}d\bar{z}.$$
 (25)

Since $\Delta z = n\epsilon$ and θ_0 is a periodic function, we can transform equation (25) into a periodic integral, which is

$$\frac{d\bar{t}_a}{d\bar{z}}|_{\bar{z}=\bar{z}_m} \frac{\Delta z}{L} \simeq \frac{n\bar{z}_m}{L} \int_0^{\epsilon} \frac{1}{(1+2\lambda)\cos(\theta_0(z)) - 1} dz = \frac{\Delta z\bar{z}_m}{\epsilon L} \int_0^{\epsilon} \frac{1}{(1+2\lambda)\cos(\theta_0(z)) - 1} dz. \tag{26}$$

By dividing equation (26) with $\Delta z/L$, we get an expression for $d\bar{t}_a/d\bar{z}$. To get \bar{t}_a , we integrate

that expression with \bar{z} running from 0 to \bar{z}_m to obtain

$$\bar{t} \simeq \bar{t}_a = \frac{\bar{z}_m^2}{2((2\lambda + 1)\cos(\theta_{ave}) - 1)}, \quad \theta_{ave} = \cos^{-1}\left(\frac{1}{2\lambda + 1}\left(\frac{\epsilon}{\int_0^{\epsilon} \frac{1}{(2\lambda + 1)\cos(\theta_0) - 1}dz} + 1\right)\right), \quad (27)$$

where θ_{ave} is a spatially averaged contact angle.

To gain further insight, we consider the simplest case where we have two different contact angles, θ_1 and θ_2 , whose fractions in one period are L_1 and L_2 , respectively. By using equation (27), we get

$$\frac{L_1}{(2\lambda+1)\cos(\theta_1)-1} + \frac{L_2}{(2\lambda+1)\cos(\theta_2)-1} = \frac{1}{(2\lambda+1)\cos(\theta_{ave})-1}.$$
 (28)

To evaluate this approximation, we compare the results from equation (28) with those from equation (23). Figures 6(a) and 6(b) show the exact and approximate relations between \bar{z}_m and \bar{t} . The approximate relation provides accurate predictions of the meniscus position in an average sense. Since the approximate solution uses an average contact angle, it does not contain the oscillations seen for some cases. We now use the simplified model (equations (27) and (28)) to explore how L_1 , θ_1 , θ_2 , and λ affect capillary filling. For simplicity, we

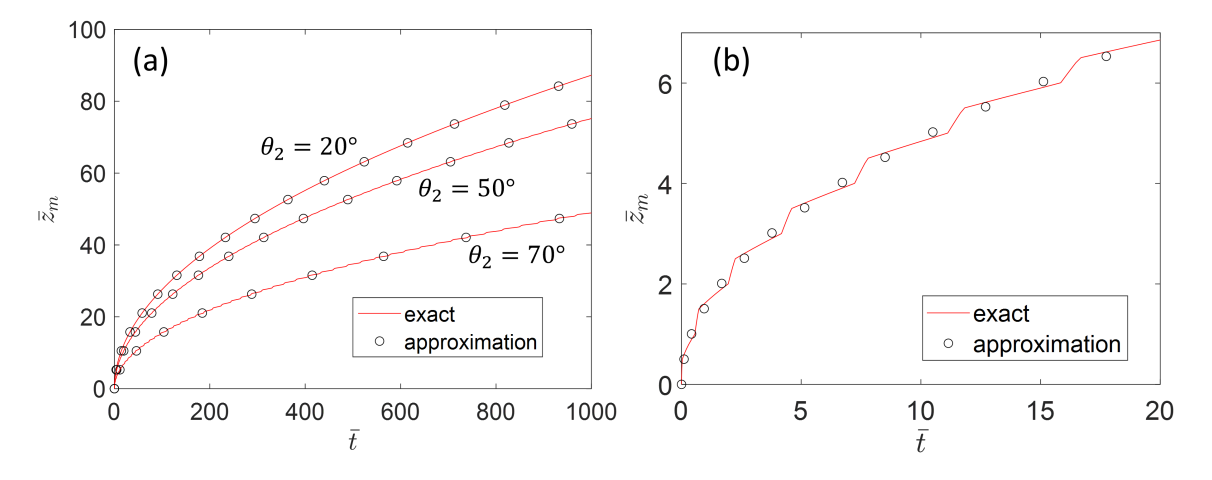


Figure 6: (a) Exact and approximate relations between \bar{z}_m and \bar{t} with different θ_2 when $\lambda = 2$, $\theta_1 = 10^\circ$, and $L_1 = 0.5$. (b) Enlargement of figure 6(a) when $\theta_2 = 70^\circ$.

consider the case where $\theta_1 < \theta_2$.

Before we explain how L_1 , θ_1 , θ_2 , and λ affect capillary filling, we need to introduce $\theta_{critical}$, the critical contact angle for which capillary flow stops. From equation (20), we see that when $\theta_0 = \cos^{-1}(1/(2\lambda+1)) = \theta_{critical}$, there is no capillary force, which means capillary filling stops. When $\lambda = 0.5$, $\theta_{critical} = 60^{\circ}$. When θ_0 approaches $\theta_{critical}$, the capillary force is almost zero and capillary filling becomes slow.

Figure 7 shows \bar{z}_m versus \bar{t} with different L_1 and θ_2 when $\lambda = 0.5$. In figure 7(a) we set $\theta_1 = 10^{\circ}$ and $\theta_2 = 55^{\circ}$. We see that because θ_2 is much larger than θ_1 , increasing L_1 enhances the velocity of capillary filling, as might be expected since the fraction of the surface having the lower contact angle increases. In figure 7(b) we set that $\theta_1 = 10^{\circ}$ and $\theta_2 = 30^{\circ}$. Here, we see that when θ_1 is close to θ_2 , increasing L_1 does not enhance the velocity of capillary filling very much compared to the case considered in figure 7(a). Thus, we conclude that the sensitivity of the velocity of capillary filling to L_1 is determined by the difference of θ_1 and θ_2 due to the capillary-force difference associated with the regions having these contact angles.

Figures 8 shows \bar{z}_m versus \bar{t} for different θ_1 and L_1 when $\theta_2 = 55^{\circ}$ and $\lambda = 0.5$. When $\lambda = 0.5$, $\theta_{critical} = 60^{\circ}$, which means θ_2 here is close to $\theta_{critical}$. From figure 8(a), we see

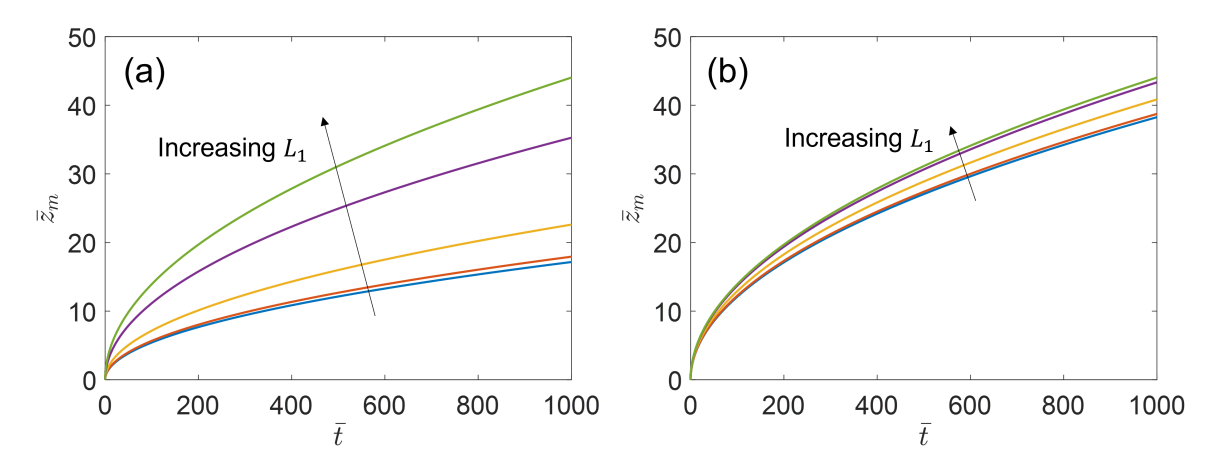


Figure 7: \bar{z}_m as a function of \bar{t} with different L_1 when $\lambda = 0.5$, $\theta_1 = 10^\circ$, and (a) $\theta_2 = 55^\circ$ and (b) $\theta_2 = 30^\circ$, where the values of L_1 are 0, 0.1, 0.5, 0.9, and 1.

that when $L_1 = 0.1$, decreasing θ_1 hardly enhances the velocity since when L_1 is small, the area with θ_1 is small. When L_1 is 0.5 or 0.9, decreasing θ_1 enhances the velocity more due to larger areas with θ_1 , as seen in figures 8(b) and 8(c). Additionally, from figures 7(a) and 8(b), we see that when θ_2 is close to $\theta_{critical}$, the velocity of capillary filling is more sensitive to L_1 than it is to θ_1 . The reason is that when θ_2 is close to $\theta_{critical}$, liquid spends a lot of time flowing through the region with θ_2 and decreasing θ_1 cannot enhance the velocity in this region. On the other hand, increasing L_1 reduces the area where liquid flows slowly and decreases the time for liquid to flow through regions with θ_2 .

Figure 9 shows relations between \bar{z}_m and \bar{t} for different θ_2 and L_1 when $\theta_1 = 10^\circ$. From figure 9(a), we see that decreasing θ_2 enhances the velocity of capillary filling. When liquid flows through regions with θ_2 , decreasing θ_2 makes the liquid front more curved and enhances

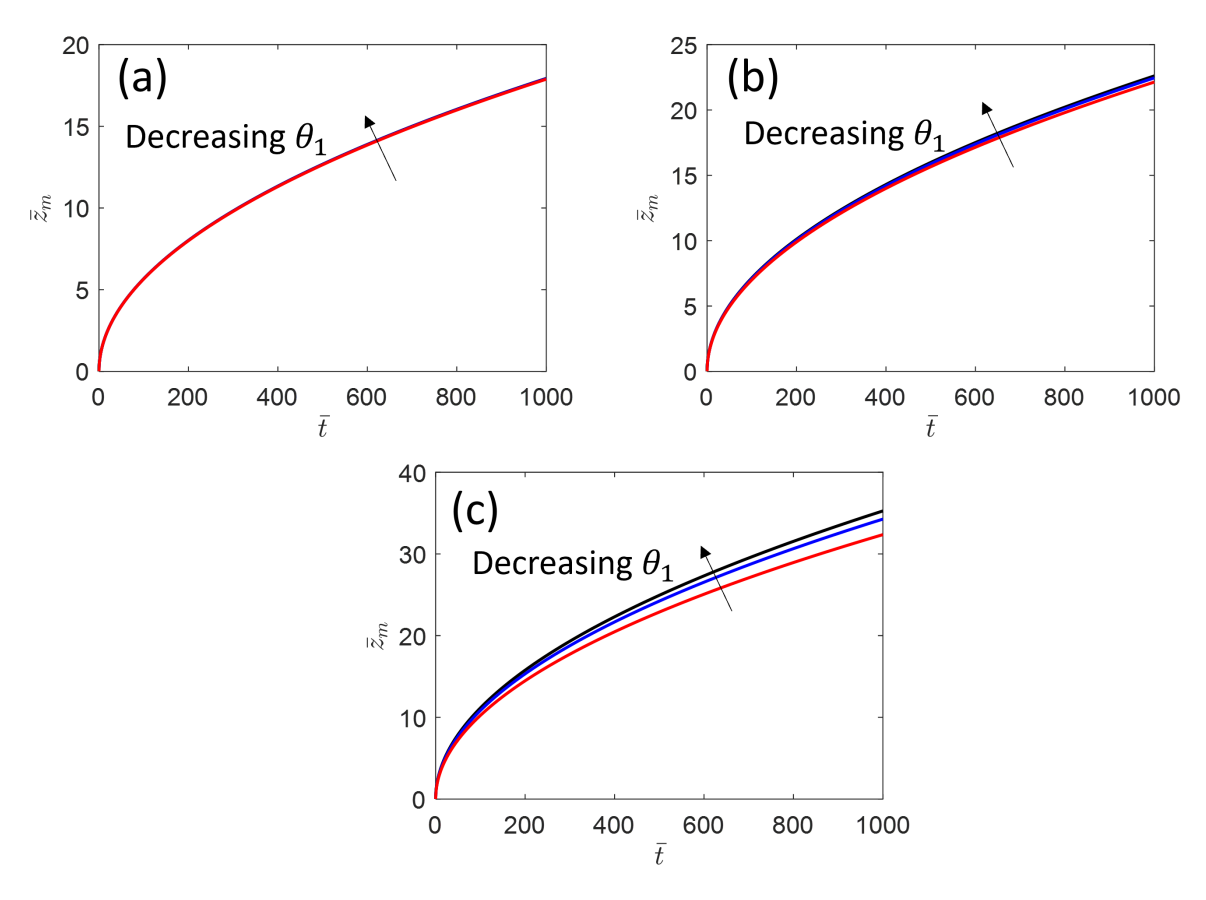


Figure 8: \bar{z}_m as a function of \bar{t} with different θ_1 when $\lambda = 0.5$, $\theta_2 = 55^\circ$, and (a) $L_1 = 0.1$, (b) $L_1 = 0.5$ and (c) $L_1 = 0.9$, where the values of θ_1 are 30°, 20°, and 10°.

the pressure difference between the liquid front and gas phase. Also, from figures 9(b) and 9(c), we see the same trend, and the only difference is the sensitivity to θ_2 due to the portion of surface with θ_2 in the open microchannel, as explained in previous paragraph. When θ_2 is larger than θ_1 , from figures 8(b) and 9(b), we see that compared with θ_1 , the velocity of capillary filling is more sensitive to θ_2 . From equation (20), we see that the capillary force is smaller in the region with θ_2 , which means compared to the region with θ_1 , liquid flows slowly in the region with θ_2 . Therefore, by decreasing θ_2 , we make the capillary force much larger so liquid flows faster.

Since we use $\xi(\lambda)$, the geometric factor due to the viscous force, to do the nondimensionalization in previous sections (see equation (23)), to know how λ changes capillary filling with periodic contact-angle variation, we need to nondimensionalize equation (27) using

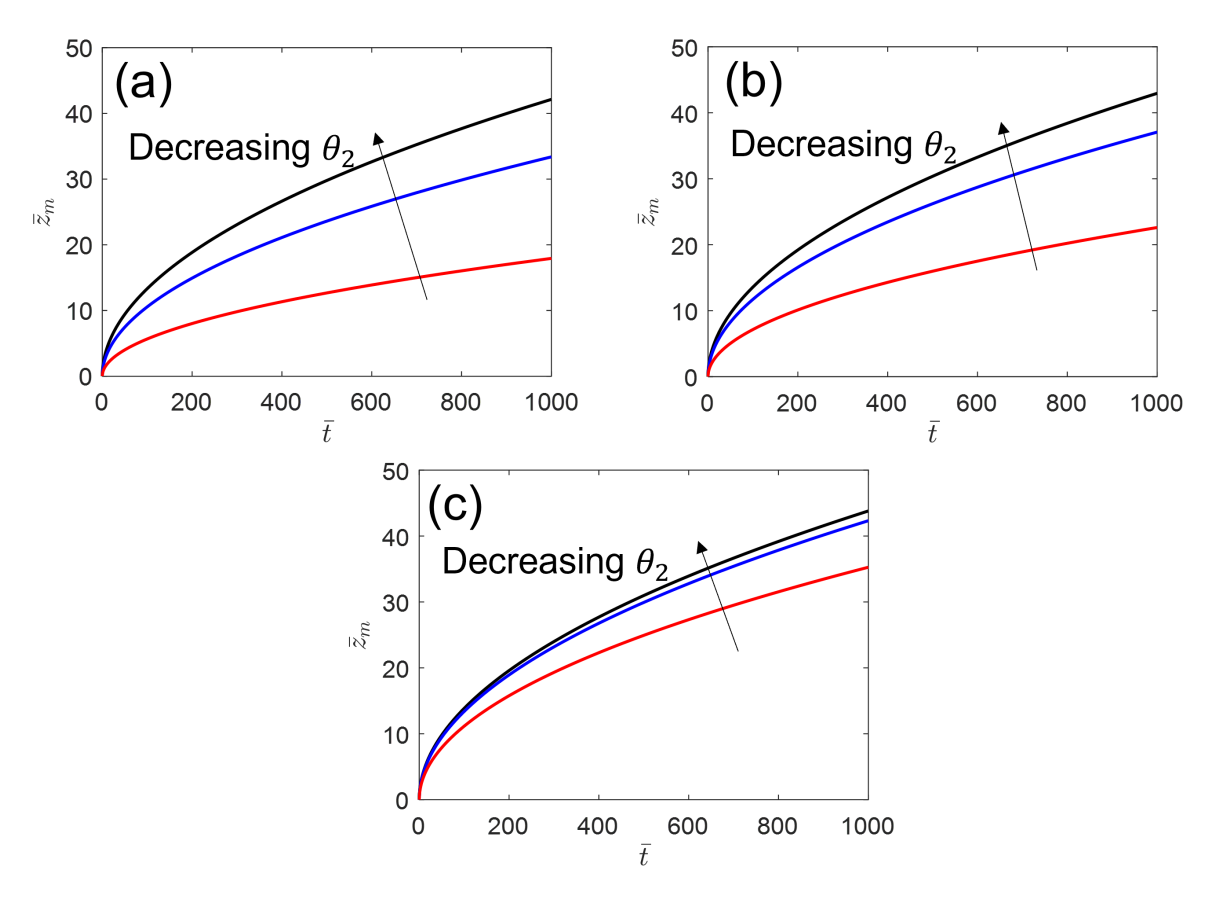


Figure 9: \bar{z}_m versus \bar{t} with different θ_2 when $\lambda = 0.5$, $\theta_1 = 10^\circ$ and (a) $L_1 = 0.1$, (b) $L_1 = 0.5$ and (c) $L_1 = 0.9$, where the values of θ_2 are 55°, 40°, and 20°.

equation (13) to include the effect of the viscous force due to different aspect ratios. For a microchannel without contact-angle variation, figure 2 shows that there is an aspect ratio where the mobility is maxmized. This reflects a balance between capillary forces, which drive flow, and viscous forces, which hinder flow. Thus changing λ can either increase or decrease the meniscus velocity, depending on the values of λ that are chosen. Figure 10 shows \bar{z}_m versus \tilde{t} for different λ and L_1 . When $L_1 = 1$, increasing λ decreases the velocity, whereas when $L_1 = 0$, increasing λ increases the velocity. When $L_1 = 0.5$, increasing λ increases the velocity for the pair of contact angles chosen. Because θ_2 is much larger than θ_1 , liquid spends much more time in regions with θ_2 . As a consequence, the behavior of the velocity with respect to λ is similar to the case where $L_1 = 0$.

Conclusions

We have developed modifications of the Lucas-Washburn model to explore how a spatially varying contact angle influences capillary flow in open rectangular microchannels. Four cases are considered: (i) different uniform contact angles on channel sidewalls and channel bottom, (ii) contact angle varying along channel cross section, and (iii) contact angle varying monotonically along channel length, and (iv) contact angle varying periodically along channel

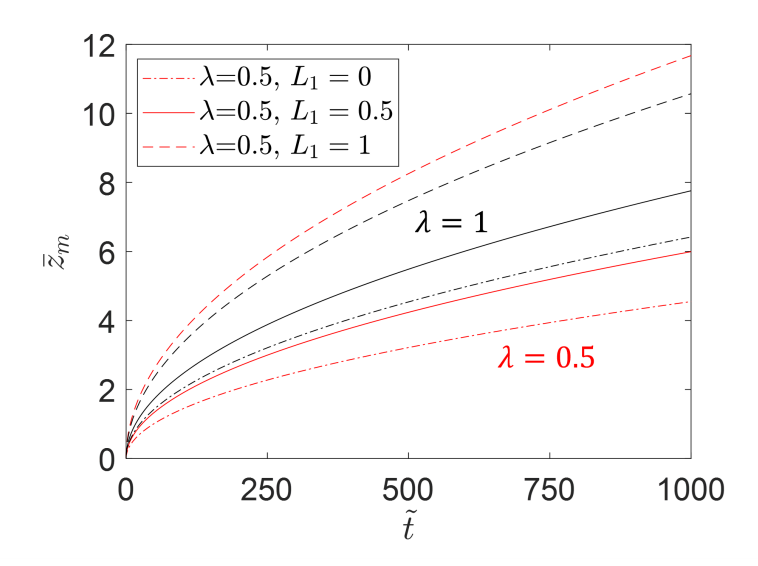


Figure 10: \bar{z}_m as a function of \bar{t} with different λ when $\theta_1 = 10^{\circ}$ and $\theta_2 = 55^{\circ}$.

length. For case (i), it is found that the maximum filling velocity is more sensitive to changes in the wall contact angle. For case (ii), the contact angles can be averaged to transform the problem to that of case (i). For case (iii), the time evolution of the meniscus position no longer follows the simple square-root law at short times. Finally, for case (iv), the problem is well described by using a uniform contact angle that is a suitable average.

Our results provide insight into earlier experiments of Xing et al. [49] by isolating the effects of wettability gradients from those of surface roughness. Our results also provide insight into how to design contact-angle variations to control capillary filling, which we hope will inspire complementary experiments to test some of the predictions made here. For example, in channels with a contact angle varying perioidcally along the channel length such that there are alternating regions of two different contact angles, we show that filling is more sensitive to certain variables than others. Since contact-angle variations can occur naturally due to surface contamination or chemical reaction, our results should be useful for understanding capillary filling in these contexts as well.

Although we have focused on open microchannels in this work because of the applications mentioned in the introduction, the approach used here can readily be exended to closed microchannels. In addition, instead of a pure liquid, one could consider a liquid solution where a solvent evpaorates and leaves behind a solute deposition pattern [54–56]. Finally, it should be noted that while Lucas-Washburn-type models make a number of simplications, their predictions are in qualitative, and sometimes quantitative, agreement with those of models that more accurately describe the shape of the liquid-gas interface [34].

Acknowledgement

This work was supported by the National Science Foundation (NSF) under grant no. CMMI-2038722. We thank Prof. Lorraine Francis for helpful discussions.

Appendix

Analytical expressions for contact-angle variation along channel length

We used equation (23) to get the time evolution of the meniscus position with different kinds of contact-angle variations along the channel length. For figure 4(a), we used

$$\theta_0 = \cos^{-1}\left(\frac{a}{1+2\lambda} + \left(\frac{c}{1+2\lambda} - \frac{c\bar{z}}{(1+\bar{z})(1+2\lambda)}\right)\right) \tag{A.1}$$

to describe the spatial variation of contact angle. In equation (A.1), we used parameter a to control the contact angle at the end of the microchannel and used parameter c to control the variation of contact angle. After substituting equation (A.1) into equation (23), we can integrate it to get

$$\bar{t} = \frac{(a-1)\bar{z}_m((a-1)\bar{z}_m - 2c) + 2c(a-1+c)\ln\left(\frac{(a-1)\bar{z}_m + a - 1 + c}{a - 1 + c}\right)}{2(a-1)^3}.$$
(A.2)

For case 1, case 2, and case 3 in figure 4(a), we used a = 3 and c = 1, 0, -1, in equation (A.2) to generate figure 4(b).

Similarly, for figure 4(c), we used

$$\theta_0 = \cos^{-1} \left(\frac{a \left(\frac{e^{\bar{z}-b}-1}{e^{\bar{z}-b}+1} - 1 \right) + c}{1+2\lambda} \right) \tag{A.3}$$

to describe the spatial variation of contact angle. In equation (A.3), we used parameters a, b, and c to control the magnitude of the variation, the position where the contact angle starts to change, and the contact angle at the end, respectively. After substituting equation

(A.3) into equation (23), we can integrate it to get

$$\bar{t} = \frac{\bar{z}_m((2a-c+1)\bar{z}_m + 4a\ln(f(\bar{z}_m)+1)) - 4a(Li_2(-f(\bar{z}_m)) - Li_2(-f(0)))}{2(2a-c+1)(c-1)},$$
(A.4)

where

$$f(z) = \frac{-2a + c - 1}{c - 1} e^{b - z}, \quad Li_2(z) = \sum_{k=1}^{k=\infty} \frac{z^k}{k^2}.$$
 (A.5)

Note that $Li_2(z)$ is the dilogarithm function [57]. For case 4, case 5, and case 6 in figure 4(c), we used a = 0.25, 0, -0.25, b = 8, and c = 2.25, 1.75, 1.25, respectively, in equation (A.4) to generate figure 4(d).

From equation (A.2), we see that there are three terms, which are \bar{z}_m^2 , \bar{z}_m and $\ln(\bar{z}_m)$. When $\bar{z}_m \gg 1$, $\bar{z}_m^2 \gg \bar{z}_m \gg \ln(\bar{z}_m)$, so for the contact-angle variations shown in figure 4, when $\bar{z}_m \gg 1$, only \bar{z}_m^2 is important to the time evolution of the meniscus position. Also, from equation (A.5), we see that when z is much larger than b, f(z) and $Li_2(-f(z))$ approach to zero. From equation (A.4), we then conclude that when $\bar{z}_m \gg b$, $z_m^2 \sim t$ at long times.

Modified Lucas-Washburn equation with inertial effects

A modified Lucas-Washburn equation with inertial effects has been derived in previous studies [54, 58]. It can be written as

$$\rho z_m HW \frac{d^2 z_m}{dt^2} + \left[1 - f_o(\lambda)\right] \rho HW \left(\frac{dz_m}{dt}\right)^2 = f_c + f_v, \tag{A.6}$$

where $f_o(\lambda)$ is a function of aspect ratio [54] and ρ is the liquid density. Non-dimensionalizing using equation (13) yields

$$\frac{4\rho\sigma H^3\bar{z}_m}{\mu^2L^2}\frac{d^2\bar{z}_m}{d\tilde{t}^2} + \frac{4\rho\sigma H^3[1 - f_o(\lambda)]}{\mu^2L^2}\left(\frac{d\bar{z}_m}{d\tilde{t}}\right)^2 = -\frac{6\bar{z}_m}{\xi(\lambda)}\frac{d\bar{z}_m}{d\tilde{t}} + ((1+2\lambda)\cos(\theta_0) - 1). \quad (A.7)$$

From equation (A.7), we see that when $\sqrt{\rho\sigma H}H/\mu L = (H/L)Oh^{-1} \ll 1$, inertial effects are negligible, where $\mu/\sqrt{\rho\sigma H}$ is the Ohnesorge number [59], which can be interpreted as

a capillary number where the characteristic velocity is the capillary wave speed. Letting $L^* = HOh^{-1}$, this implies that inertial effects are negligible when $L^*/L \ll 1$. So, if the channel length or length scale of wettability variation is much larger than L^* , inertial effects can be neglected [60].

References

- (1) Wheeler, A. R.; Throndset, W. R.; Whelan, R. J.; Leach, A. M.; Zare, R. N.; Liao, Y. H.; Farrell, K.; Manger, I. D.; Daridon, A. Microfluidic device for single-cell analysis. Anal. Chem. 2003, 75, 3581–3586.
- (2) Yang, S.; Ündar, A.; Zahn, J. D. A microfluidic device for continuous, real time blood plasma separation. *Lab Chip* **2006**, *6*, 871–880.
- (3) Jia, J.; Song, Q.; Liu, Z.; Wang, B. Effect of wall roughness on performance of microchannel applied in microfluidic device. *Microsyst. Technol.* **2019**, *25*, 2385–2397.
- (4) Kee, R. J.; Almand, B. B.; Blasi, J. M.; Rosen, B. L.; Hartmann, M.; Sullivan, N. P.; Zhua, H.; Manerbino, A. R.; Menzer, S.; Coors, W. G.; Martin, J. L. The design, fabrication, and evaluation of a ceramic counter-flow microchannel heat exchanger. Appl. Therm. Eng. 2011, 31, 2004–2012.
- (5) Hasan, M. I.; Rageb, A. A.; Yaghoubi, M.; Homayoni, H. Influence of channel geometry on the performance of a counter flow microchannel heat exchanger. *Int. J. Therm. Sci.* 2009, 48, 1607–1618.
- (6) Arie, M. A.; Shooshtari, A. H.; Dessiatoun, S. V.; Al-Hajri, E.; Ohadi, M. M. Numerical modeling and thermal optimization of a single-phase flow manifold-microchannel plate heat exchanger. *Int. J. Heat Mass Transfer* 2015, 81, 478–489.
- (7) Zhang, X.; Stefanick, S.; Villani, F. J. Application of microreactor technology in process development. *Org. Process Res. Dev.* **2004**, *8*, 455–460.
- (8) Ahmed-Omer, B.; Brandt, J. C.; Wirth, T. Advanced organic synthesis using microre-actor technology. *Org. Biomol. Chem.* **2007**, *5*, 733–740.
- (9) Miyazaki, M.; Maeda, H. Microchannel enzyme reactors and their applications for processing. *Trends Biotechnol.* **2006**, *24*, 463–470.
- (10) He, Y.; Kim, K.; Chang, C. Continuous, size and shape-control synthesis of hollow silica nanoparticles enabled by a microreactor-assisted rapid mixing process. *Nanotechnology* **2017**, *28*, 235602.

- (11) Ducry, L.; Roberge, D. M. Controlled autocatalytic nitration of phenol in a microre-actor. *Angew. Chem. Int. Ed.* **2005**, *44*, 7972–7975.
- (12) Liu, Z.; Lu, Y.; Yang, B.; Luo, G. Controllable preparation of poly(butyl acrylate) by suspension polymerization in a coaxial capillary microreactor. *Ind. Eng. Chem. Res.* 2011, 50, 11853–11862.
- (13) Harpole, G. M.; Eninger, J. E. In *Proceeding of the 7th IEEE SEMI-THERM Symposium*, 1991, pp 59–63.
- (14) Tsuzuki, N.; Kato, Y.; Nikitin, K.; Ishizuka, T. Advanced microchannel heat exchanger with s-shaped fins. *J Nucl Sci Technol* **2009**, *46*, 403–412.
- (15) Ashman, S.; Kandlikar, S. G. In *International Conference on Nanochannels, Microchannels, and Minichannels*, 2006; Vol. 47608, pp 855–860.
- (16) Jochem, K. S.; Suszynski, W. J.; Frisbie, C. D.; Francis, L. F. High-Resolution, high-aspect-ratio printed and plated metal conductors utilizing roll-to-roll microscale UV imprinting with prototype imprinting stamps. *Ind. Eng. Chem. Res.* 2018, 57, 16335–16346.
- (17) Cao, M.; Jochem, K.; Hyun, W. J.; Francis, L. F.; Frisbie, C. D. Self-aligned inkjet printing of resistors and low-pass resistor–capacitor filters on roll-to-roll imprinted plastics with resistances ranging from 10 to 10⁶ Ω. Flexible Printed Electron. 2018, 3, 045003.
- (18) Lauri, J.; Liedert, C.; Liedert, R.; Fabritius, T. In 2020 IEEE International Instrumentation and Measurement Technology Conference (I2MTC), 2020, pp 1–5.
- (19) Subramanian, V.; Frchet, J. M. J.; Chang, P.; Huang, D.; Lee, J.; Molesa, S.; Murphy, A.; Redinger, D.; Volkman, S. Progress toward development of all-printed RFID tags: materials, processes, and devices. *Proc. IEEE* 2005, 93, 1330–1338.
- (20) Khan, Y.; Ostfeld, A. E.; Lochner, C. M.; Pierre, A.; Arias, A. C. Monitoring of vital signs with flexible and wearable medical devices. *Adv. Mater.* **2016**, *28*, 4373–4395.

- (21) Chang, W.; Fang, T.; Shen, Y.; Lin, Y. Flexible electronics sensors for tactile multi-scanning. *Rev. Sci. Instrum.* **2009**, *80*, 084701.
- (22) Nilson, R. H.; Tchikanda, S. W.; Griffiths, S. K.; Martinez, M. J. Steady evaporating flow in rectangular microchannels. *Int. J. Heat Mass Transfer* **2006**, *49*, 1603–1618.
- (23) Xia, Z. Z.; Yang, G. Z.; Wang, R. Z. Capillary-assisted flow and evaporation inside circumferential rectangular micro groove. *Int. J. Heat Mass Transfer* **2009**, *52*, 952–961.
- (24) Lee, J. K.; Kung, M. C.; Kung, H. H.; Mockros, L. F. Microchannel technologies for artificial lungs: (3) open rectangular channels. *ASAIO J.* **2008**, *54*, 390–395.
- (25) Yang, D.; Krasowska, M.; Priest, C.; Popescu, M. N.; Ralston, J. Dynamics of capillary-driven flow in open microchannels. *J. Phys. Chem. C* **2011**, *115*, 18761–18769.
- (26) Lucas, R. Ueber das Zeitgesetz des kapillaren Aufstiegs von Flüssigkeiten. *Kolloid-Z* 1918, 23, 15–22.
- (27) Washburn, E. W. The dynamics of capillary flow. Phys. Rev. 1921, 17, 273–283.
- (28) Cai, J.; Chen, Y.; Liu, Y.; Li, S.; Sun, C. Capillary imbibition and flow of wetting liquid in irregular capillaries: A 100-year review. *Adv. Colloid Interface Sci.* **2022**, 304, 102654.
- (29) Cai, J.; Jin, T.; Kou, J.; Zou, S.; Xiao, J.; Meng, Q. Lucas–Washburn equation-based modeling of capillary-driven flow in porous systems. *Langmuir* **2021**, *37*, 1623–1636.
- (30) Lee, J. J.; Berthier, J.; Theberge, A. B.; Berthier, E. Capillary flow in open microgrooves: bifurcations and networks. *Langmuir* **2019**, *35*, 10667–10675.
- (31) Keshmiri, K.; Huang, H.; Jemere, A. B.; Nazemifard, N. Investigation of capillary filling dynamics of multicomponent fluids in straight and periodically constricted microchannels. *Langmuir* **2020**, *36*, 6304–6313.
- (32) Chen, G.-L.; He, G.-Y.; Sheng, Y.-J.; Tsao, H.-K. Imbibition dynamics in a u-groove microchannel with sudden enlargement. *Langmuir* **2023**, *39*, 10993–11002.

- (33) Garcia Eijo, P. M.; Cabaleiro, J. M.; Artana, G. Capillary flow dynamics in composite rectangular microchannels with rough walls. *Langmuir* **2022**, *38*, 13296–13304.
- (34) Kolliopoulos, P.; Jochem, K. S.; Johnson, D.; Suszynski, W. J.; Francis, L. F.; Kumar, S. Capillary-flow dynamics in open rectangular microchannels. J. Fluid Mech. 2021, 911, A32.
- (35) Gau, H.; Herminghaus, S.; Lenz, P.; Lipowsky, R. Liquid morphologies on structured surfaces: From microchannels to microchips. *Science* **1999**, *283*, 46–49.
- (36) Lu, Y.; Shen, Y.; Tao, J.; Wu, Z.; Chen, H.; Jia, Z.; Xu, Y.; Xie, X. Droplet directional movement on the homogeneously structured superhydrophobic surface with the gradient non-wettability. *Langmuir* **2020**, *36*, 880–888.
- (37) Chu, F.; Luo, J.; Hao, C.; Zhang, J.; Wu, X.; Wen, D. Directional transportation of impacting droplets on wettability-controlled surfaces. *Langmuir* **2020**, *36*, 5855–5862.
- (38) Lowrey, S.; Misiiuk, K.; Blaikie, R.; Sommers, A. Survey of micro/nanofabricated chemical, topographical, and compound passive wetting gradient surfaces. *Langmuir* **2021**, *38*, 605–619.
- (39) Li, J.; Zhou, Y.; Cong, J.; Xu, C.; Ren, L. Bioinspired integrative surface with hierarchical texture and wettable gradient-driven water collection. *Langmuir* **2020**, *36*, 14737–14747.
- (40) Ji, J.; Jiao, Y.; Song, Q.; Zhang, Y.; Liu, X.; Liu, K. Bioinspired geometry-gradient metal slippery surface by one-step laser ablation for continuous liquid directional self-transport. *Langmuir* **2021**, *37*, 5436–5444.
- (41) Misiiuk, K.; Lowrey, S.; Blaikie, R.; Juras, J.; Sommers, A. Development of a coating-less aluminum superhydrophobic gradient for spontaneous water droplet motion using one-step laser-ablation. *Langmuir* **2022**, *38*, 1954–1965.
- (42) Calvert, J. M. Lithographic patterning of self-assembled films. J. Vac. Sci. Technol. B 1993, 11, 2155–2163.

- (43) Abate, A. R.; Krummel, A. T.; Lee, D.; Marquez, M.; Holtze, C.; Weitz, D. A. Photore-active coating for high-contrast spatial patterning of microfluidic device wettability.

 *Lab Chip 2008, 8, 2157–2160.
- (44) Tian, D.; Song, Y.; Jiang, L. Patterning of controllable surface wettability for printing techniques. *Chem. Soc. Rev.* **2013**, *42*, 5184–5209.
- (45) Abbott, N. L.; Folkers, J. P.; Whitesides, G. M. Manipulation of the wettability of surfaces on the 0.1- to 1 -micrometer scale through micromachining and molecular self-assembly. *Science* **1992**, *257*, 1380–1382.
- (46) Matsumura, T.; Iida, F.; Hirose, T.; Yoshino, M. Micro machining for control of wettability with surface topography. *J. Mater. Process. Technol.* **2012**, *212*, 2669–2677.
- (47) O'Loughlin, M.; Priest, C.; Popescu, M. N.; Ralston, J. Patterning of wettability for controlling capillary-driven flow in closed channels. J. Colloid Interface Sci. 2013, 402, 259–266.
- (48) Suk, J. W.; Cho, J.-H. Capillary flow control using hydrophobic patterns. *J. Micromech. Microeng.* **2007**, *17*, N11–N15.
- (49) Xing, H.; Cheng, J.; Zhou, C. Effect of gradient wettability on capillary imbibition in open semicircular copper channel. *Phys. Fluids* **2020**, *32*, 112004.
- (50) Oron, A.; Davis, S. H.; Bankoff, S. G. Long-scale evolution of thin liquid films. Rev. Mod. Phys. 1997, 69, 931–980.
- (51) Ouali, F. F.; McHate, G.; Javed, H.; Trabi, C.; Shirtcliffe, N. J.; Newton, M. I. Wetting considerations in capillary rise and imbibition in closed square tubes and open rectangular cross-section channels. *Microfluid. Nanofluid.* **2013**, *15*, 309–326.
- (52) Good, R. J. The rate of penetration of a fluid into a porous body initially devoid of adsorbed material (1, 2). *J. Colloid Interface Sci.* **1973**, 42, 473–477.
- (53) Cassie, A. B. D.; Baxter, S. Wettability of porous surfaces. *Trans. Faraday Soc.* **1944**, 40, 546–551.

- (54) Kolliopoulos, P.; Jochem, K. S.; Johnson, D.; Suszynski, W. J.; Francis, L. F.; Kumar, S. Capillary flow with evaporation in open rectangular microchannels. *Langmuir* 2019, 35, 8131–8143.
- (55) Kolliopoulos, P.; Jochem, K. S.; Francis, L. F.; Kumar, S. Capillary flow of evaporating liquid solutions in open rectangular microchannels. *J. Fluid Mech.* **2022**, *938*, A22.
- (56) Kolliopoulos, P.; Kumar, S. Capillary flow of liquids in open microchannels: overview and recent advances. *NPJ Microgravity* **2021**, *7*, 51.
- (57) Zagier, D. In Frontiers in Number Theory, Physics, and Geometry II: On Conformal Field Theories, Discrete Groups and Renormalization; Springer: 2007, pp 3–65.
- (58) Bosanquet, C. H. LV. On the flow of liquids into capillary tubes. *London. Edinb. Dublin philos. maq. j. sci.* **1923**, 45, 525–531.
- (59) McKinley, G. H.; Renardy, M. Wolfgang von Ohnesorge. *Phys. Fluids* **2011**, *23*, 127101.
- (60) Das, S.; Waghmare, P. R.; Mitra, S. K. Early regimes of capillary filling. *Phys. Rev.* E 2012, 86, 067301.

TOC Graphic

